Vol. **113** (2008) *ACTA PHYSICA POLONICA A* No. 6

# Measurement of *L* Shell X-Ray Production and Average *L* Shell Fluorescence Yields for Some Heavy Elements at 123.6 keV

G. Apaydin*, V. Aylikçi, N. Kaya, E. Cengiz and E. Tiraşoğlu

Department of Physics, Faculty of Arts and Sciences
Karadeniz Technical University, 61080, Trabzon, Turkey

*(Received March 4, 2008; in final form April 9, 2008)*

The $L_{3l}$, $L_{3\alpha}$, $L_{3\beta}$, $L_{2\beta}$, $L_{2\gamma}$, $L_{2\eta}$, $L_{1\beta}$ and $L_{1\gamma}$ X-ray production cross-sections and $L$ shell average fluorescence yields were measured for the elements from Re to U using excitation energy of 123.6 keV. Measurements were performed using an $^{57}$Co annular radioactive source and a Si(Li) detector. The theoretical values of the cross-sections were calculated using theoretically tabulated values of subshell photoionization cross-sections; the Coster–Kronig transition probabilities were based on the Dirac–Hartree–Slater theory and radiative emission rates. Experimental results were compared with the theoretically calculated values of $L$ shell X-ray cross-sections. The present experimental results are in agreement with theoretical values.

PACS numbers: 32.30.Rj, 32.50.+d, 32.80.Fb

## 1. Introduction

Reliable values of $L$ X-ray production cross-sections are important in the study of some basic phenomena in atomic, molecular and radiation physics and in non-destructive trace element analysis of variety samples using energy dispersive X-ray fluorescence (ED-XRF) method. Also, comparison of measured cross-sections with theoretical estimates provides a check on validity of various physical parameters such as photoionization cross-section and fluorescence yield involved in the evaluation of theoretical estimation. A review of the literature shows that a number of experimental studies on the $L$ shell reported more than other

*corresponding author; e-mail: gapaydin@ktu.edu.tr

shells, because of the prevalent irradiated energies could be excited for most elements. Numerous experiments have been carried out to measure $L$ X-ray cross--sections using $^{241}$Am radioactive source (at the excitation energy 59.543 keV) in different elements [1–13]. Some experimental studies were carried out using secondary target irradiated by $^{241}$Am radioactive source [14–18]. Garg et al. [19] measured $L$ X-ray fluorescence cross-sections for elements in the atomic range $41 \leq Z \leq 52$ at 5.96 keV energy. $L_{\gamma 1,5}$, $L_{\gamma 2,3,(6)}$, $L_{\gamma 4}$ and $L_{\alpha}$ X-ray fluorescence cross-sections for the elements with $71 \leq Z \leq 83$ at 22.6 keV have been measured by Puri et al. [20]. Doğan et al. [21] have measured $L_l$, $L_{\alpha}$, $L_{\beta}$ and $L_{\gamma}$ X-ray fluorescence cross-sections using two different energies 59.5 and 123.6 keV. In some studies, targets were excited with X-ray tube [22–26], protons [27–30], electrons [31–33] and ions [34–37] as an alternative to radioisotopes.

In the present investigation, the $L$ subshell cross-sections ($\sigma_{Li}^{\mathrm{X}}(i = \ell, \eta, \alpha_{1,2}, \beta_{1,2,6,15}, \gamma_{1,2,3,5})$) and $L$ shell average fluorescence yields ($\varpi_L$) for elements in the range $75 \leq Z \leq 92$ have been measured for 123.6 keV energy. Comparisons have been made of the experimental results with calculated theoretical values and theoretical results.

## 2. Experimental

The geometry of the experimental setup for our annular source used in the X-ray fluorescence analysis is shown in Fig. 1. Pure heavy elements and their compounds were used as samples. Indicated elements were supplied commercially by Aldrich and Alfa Aesar. Purity of the elements was better than 98%. Powder samples were sieved with 400 mesh and supporting on mylar film at 20–40 mg/cm$^2$ mass thickness. All samples were irradiated by 123.6 keV photons emitted by an annular 925 MBq $^{57}$Co radioisotope source. (The radioactive source $^{57}$Co decays by electron conversion process into metastable states of $^{57}$Fe and in turn into $\gamma$ photons of energies 122 (85%), 136 (11%), and 14.4 keV (8.5%). Since the intensity of the 122 keV photons is predominant over that of the 136 keV photons and as they are close to each other, we can take the weighted average of 122 keV and 136 keV, i.e. 123.6 keV.) A detailed description of the present experimental equipments has been explained in our previous work [38].

In the experimental determinations, spectral deconvolution is one of the main problems that arise when determining these parameters due to the strong peak overlapping in ED-XRF system. Good statistics is not enough for this purpose and a careful fitting methodology is required in order to obtain accurate values for the peak areas. Conventional fitting programs have not shown good performance, but the method of parameter optimization was previously developed for X-ray fluorescence analysis. In the present work, a new peak fitting program which was developed by Origin Company (Origin 7.0) was used to determine accurate peak intensity. In the present study, Fig. 2 shows the spectra of $K$ and $L$ X-rays for thorium.

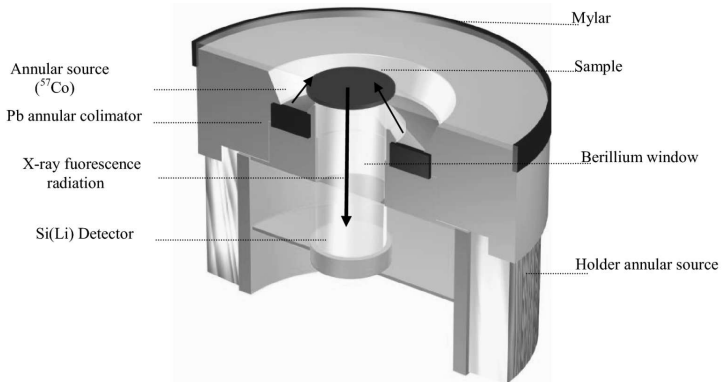


Fig. 1. Geometry of the experimental setup.

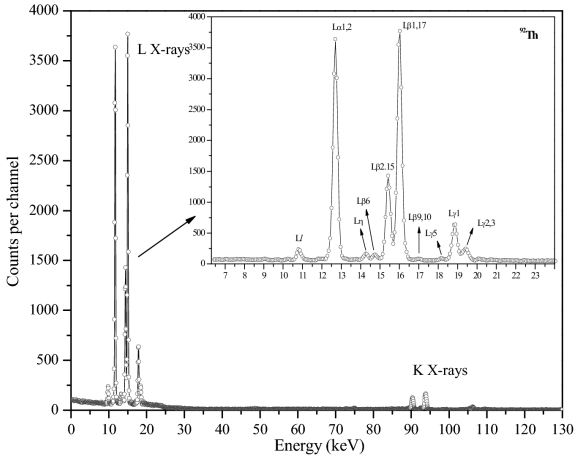


Fig. 2. Thorium $K$ and $L$ X-rays spectrum, using $^{57}$Co source.

## 3. Data analysis

The experimental $Li$ X-ray production cross-sections are evaluated using the relation

$$\sigma_{Li}^{\mathrm{X}} = \frac{N_{Li}}{I_0 G \varepsilon_{Li} \beta_{Li} t}, \tag{1}$$

where $N_{Li}$ $(i = \ell, \eta, \alpha_{1,2}, \beta_{1,2,6,9,10,15,17}, \gamma_{1,2,3,5})$ is the net counts per unit time under the associated elemental photopeak, $I_0 G$ is the intensity of exciting radiation falling on sample, $\varepsilon$ is the detector efficiency for the $L_i$ X-rays of the element, $t$ is the thickness of target in g/cm$^2$ and $\beta_{Li}$ is the self-absorption given by

$$\beta = \frac{1 - \exp\left(-\left(\frac{\mu_{\mathrm{p}}}{\cos\theta_1} + \frac{\mu_{\mathrm{e}}}{\cos\theta_2}\right) t\right)}{\left(\frac{\mu_{\mathrm{p}}}{\cos\theta_1} + \frac{\mu_{\mathrm{e}}}{\cos\theta_2}\right) t}, \tag{2}$$

where $\mu_{\mathrm{p}}$ and $\mu_{\mathrm{e}}$ are the total mass absorption coefficients of target material at the

incident photon energy and at the emitted average $L_i$ X-ray energy (from XCOM [39]), $\theta_1$ and $\theta_2$ are the angles of incident photon and emitted X-rays with respect to the normal at the surface of the sample, respectively.

Semi-empirical average $L$ shell fluorescence yields were obtained using the following equation:

$$\varpi_L = \frac{\sigma_L^{\mathrm{X}}}{\sigma_L^{\mathrm{P}} + \eta_{KL} + \sigma_K^{\mathrm{P}}}, \tag{3}$$

where $\sigma_K^{\mathrm{P}}$ and $\sigma_L^{\mathrm{P}}$ are $K$ and $L$ shell photoionization cross-sections [40], $\eta_{KL}$ is the $K$ to $L$ shell vacancy transfer probability [40] and $\sigma_L^{\mathrm{X}}$ is total $L$ shell X-ray production cross-section and it is given by

$$\sigma_L^{\mathrm{X}} = \sum_i \sigma_{Li}^{\mathrm{X}} \quad (i = \ell, \eta, \alpha_{1,2}, \beta_{1,2,6,9,10,15,17}, \gamma_{1,2,3,5}). \tag{4}$$

$\sigma_{Li}^{\mathrm{X}}$ values were determined using Eq. (1).

The product $I_0 G \varepsilon_{Li}$, containing the terms related to the incident photon flux, geometrical factor and absolute efficiency of X-ray detector, was determined by collecting the $K_\alpha$ and $K_\beta$ X-ray spectra of samples of Ce, Nd, Gd, Dy, Er, Yb, Ta, Ir, Hg, Bi, Th, and U for $^{57}$Co in the same geometry using Eq. (1) [41].

## 4. Theoretical method

The $L$ shell X-ray cross-sections are theoretically calculated by using the following equations [27]:

$$\sigma_{L3\ell}^{\mathrm{X}} = \omega_3 \left[ \left( \sigma_{L1}^{\mathrm{P}} + \sigma_K^{\mathrm{P}} \eta_{KL1} \right) \left( f_{12} f_{23} + f_{13} \right) + \left( \sigma_{L2}^{\mathrm{P}} + \sigma_K^{\mathrm{P}} \eta_{KL2} \right) f_{23} + \left( \sigma_{L3}^{\mathrm{P}} + \sigma_K^{\mathrm{P}} \eta_{KL3} \right) \right] F_{3l}, \tag{5}$$

$$\sigma_{L3\alpha_{1,2}}^{\mathrm{X}} = \omega_3 \left[ \left( \sigma_{L1}^{\mathrm{P}} + \sigma_K^{\mathrm{P}} \eta_{KL1} \right) \left( f_{12} f_{23} + f_{13} \right) + \left( \sigma_{L2}^{\mathrm{P}} + \sigma_K^{\mathrm{P}} \eta_{KL2} \right) f_{23} + \left( \sigma_{L3}^{\mathrm{P}} + \sigma_K^{\mathrm{P}} \eta_{KL3} \right) \right] F_{3\alpha}, \tag{6}$$

$$\sigma_{L3\beta_{2,6,15}}^{\mathrm{X}} = \omega_3 \left[ \left( \sigma_{L1}^{\mathrm{P}} + \sigma_K^{\mathrm{P}} \eta_{KL1} \right) \left( f_{12} f_{23} + f_{13} \right) + \left( \sigma_{L2}^{\mathrm{P}} + \sigma_K^{\mathrm{P}} \eta_{KL2} \right) f_{23} + \left( \sigma_{L3}^{\mathrm{P}} + \sigma_K^{\mathrm{P}} \eta_{KL3} \right) \right] F_{3\beta}, \tag{7}$$

$$\sigma_{L2\beta_{1,17}}^{\mathrm{X}} = \omega_2 \left[ \left( \sigma_{L1}^{\mathrm{P}} + \sigma_K^{\mathrm{P}} \eta_{KL1} \right) f_{12} + \left( \sigma_{L2}^{\mathrm{P}} + \sigma_K^{\mathrm{P}} \eta_{KL2} \right) \right] F_{2\beta}, \tag{8}$$

$$\sigma_{L2\gamma_{1,5}}^{\mathrm{X}} = \omega_2 \left[ \left( \sigma_{L1}^{\mathrm{P}} + \sigma_K^{\mathrm{P}} \eta_{KL1} \right) f_{12} + \left( \sigma_{L2}^{\mathrm{P}} + \sigma_K^{\mathrm{P}} \eta_{KL2} \right) \right] F_{2\gamma}, \tag{9}$$

$$\sigma_{L2\eta}^{\mathrm{X}} = \omega_2 \left[ \left( \sigma_{L1}^{\mathrm{P}} + \sigma_K^{\mathrm{P}} \eta_{KL1} \right) f_{12} + \left( \sigma_{L2}^{\mathrm{P}} + \sigma_K^{\mathrm{P}} \eta_{KL2} \right) \right] F_{2\eta}, \tag{10}$$

$$\sigma_{L1\beta_{9,10}}^{\mathrm{X}} = \omega_1 \left( \sigma_{L1}^{\mathrm{P}} + \sigma_K^{\mathrm{P}} \eta_{KL1} \right) F_{1\beta}, \tag{11}$$

$$\sigma_{L1\gamma_{2,3}}^{\mathrm{X}} = \omega_1 \left( \sigma_{L1}^{\mathrm{P}} + \sigma_K^{\mathrm{P}} \eta_{KL1} \right) F_{1\gamma}, \tag{12}$$

$$F_{3l} = \frac{\Gamma_{3\ell}}{\Gamma_3}, \quad F_{3\alpha} = \frac{\Gamma_{3\alpha 1} + \Gamma_{3\alpha 2}}{\Gamma_3}, \quad F_{3\beta} = \frac{\Gamma_{3\beta 2} + \Gamma_{3\beta 6} + \Gamma_{3\beta 15}}{\Gamma_3},$$

$$F_{2\beta} = \frac{\Gamma_{2\beta 1}}{\Gamma_2}, \quad F_{2\gamma} = \frac{\Gamma_{2\gamma 1} + \Gamma_{2\gamma 5}}{\Gamma_2}, \quad F_{2\eta} = \frac{\Gamma_{2\eta}}{\Gamma_2},$$
$$F_{1\beta} = \frac{\Gamma_{1\beta 9} + \Gamma_{1\beta 10}}{\Gamma_1}, \quad F_{1\gamma} = \frac{\Gamma_{1\gamma 2} + \Gamma_{1\gamma 3}}{\Gamma_1}, \tag{13}$$

where $\sigma^{\mathrm{P}}_{Li}$ ($i = 1, 2, 3$) $L$ subshell and $\sigma^{\mathrm{P}}_{K}$ $K$ shell photoionization cross-sections [40], $\omega_i$ ($i = 1, 2, 3$) is the $L$ subshell fluorescence yield [42], $\eta_{KLi}$ ($i = 1, 2, 3$) are the vacancy probabilities of $K$ to $L_i$ [43], $f_{ij}$ ($i \neq j = 1, 2, 3$) is the Coster–Kronig transition probabilities. $F_{3l}$, $F_{3\alpha}$, $F_{3\beta}$, $F_{2\beta}$, $F_{2\gamma}$, $F_{2\eta}$, $F_{1\beta}$ and $F_{1\gamma}$ are the fraction of the radiation transition of the subshell $L_i$ and $\Gamma_i$ ($i = 1, 2, 3$) is the total radiative width of $L_i$ subshell [44] and $\Gamma_{3\alpha 1}$ is the radiative transition rates contributing to $L_{\alpha 1}$ lines associated with the hole filling in the $L_3$ shell. That is

$$\Gamma_{\alpha 1} = \Gamma_3(M_5 - L_3), \quad \Gamma_{3\alpha 2} = \Gamma_3(M_4 - L_3), \quad \Gamma_{3l} = \Gamma_3(M_1 - L_3),$$
$$\Gamma_{\beta 2} = \Gamma_3(N_5 - L_3), \quad \Gamma_{3\beta 15} = \Gamma_3(N_4 - L_3), \quad \Gamma_{3\beta 6} = \Gamma_3(N_1 - L_3), \tag{14}$$
$$\Gamma_{2\beta 1} = \Gamma_2(M_4 - L_2), \quad \Gamma_{2\beta 17} = \Gamma_2(M_3 - L_2), \quad \Gamma_{2\eta} = \Gamma_2(M_1 - L_2),$$
$$\Gamma_{2\gamma 1} = \Gamma_2(N_4 - L_2), \quad \Gamma_{2\gamma 5} = \Gamma_2(N_1 - L_2), \tag{15}$$
$$\Gamma_{1\beta 9} = \Gamma_1(M_5 - L_1), \quad \Gamma_{1\beta 10} = \Gamma_1(M_4 - L_1),$$
$$\Gamma_{1\gamma 2} = \Gamma_1(N_2 - L_1), \quad \Gamma_{1\gamma 3} = \Gamma_1(N_3 - L_1), \tag{16}$$

where $\Gamma_{1\beta}$, $\Gamma_{1\gamma}$ are the radiative transition rates from the ($M_4$, $M_5$), ($N_2$, $N_3$) to the $L_1$ shell, $\Gamma_{2\eta}$, $\Gamma_{2\beta}$, $\Gamma_{2\gamma}$ are the radiative transition rates from the ($M_1$, $M_3$, $M_4$), ($N_1$, $N_4$) to the $L_2$ shell and $\Gamma_{3l}$, $\Gamma_{3\alpha}$, $\Gamma_{3\beta}$ are the radiative transition rates from the ($M_1$, $M_4$, $M_5$), ($N_1$, $N_4$, $N_5$), to the $L_3$ shell, respectively. Scofield who applied the relativistic Hartree–Slater theory with a central potential and included the retardation effect has calculated the radiative transition rates for many elements [44, 45].

## 5. Result and discussion

The measured values of $L$ shell X-ray production cross-sections for Re, Os, Ir, Pt, Au, Hg, Tl, Pb, Bi, Th and U at 123.6 keV excitation energy are given in Table I.

The experimental values of X-ray production cross-sections of $L_{3l}$, $L_{3\alpha}$, $L_{3\beta}$, $L_{2\beta}$, $L_{2\gamma}$, $L_{2\eta}$, $L_{1\beta}$ and $L_{1\gamma}$ agree to within (2.5–9.8%), (1.3–6.6%), (15–18%), (0.1–7.7%), (1.1–13%), (3.5–26.8%), (22–25%) and (15.5–40%) calculated values using Eqs. (5)–(12), respectively. While the $L_{3l}$, $L_{3\alpha}$, $L_{2\beta}$ and $L_{2\gamma}$ were observed in the all elements studied, the $L_{3\beta}$, $L_{2\eta}$, $L_{1\beta}$ and $L_{1\gamma}$ were observed in some elements. This situation is related to detector resolution.

The empirical values of the $L$ shell average fluorescence yields were shown together with the theoretical values in Table II. These values have been plotted as a function of the atomic number as shown in Fig. 3. Our empirical values agree within (4–30%), (6.6–23.5%) with the theoretical values of the Bambynek et al. [46], and Mitchell and Barfoot [47], respectively. The empirical values also

TABLE I

$L$ X-rays productions cross-sections.

| Element | $\sigma_{L_{3l}}$ $(l)$ | | $\sigma_{L_{3\alpha}}$ $(\alpha_{1.2})$ | | $\sigma_{L_{3\beta}}$ $(\beta_{2.6.15})$ | | $\sigma_{L_{2\beta}}$ $(\beta_{1.17})$ | |
|---|---|---|---|---|---|---|---|---|
| | Exp. | Theor. | Exp. | Theor. | Exp. | Theor. | Exp. | Theor. |
| $^{75}$Re | 3.33 | 3.48 | 80.73 | 82.33 | – | – | 48.48 | 50.36 |
| | ±0.13 | | ±3.23 | | | | ±1.94 | |
| $^{76}$Os | 3.59 | 3.89 | 94.36 | 95.67 | – | – | 52.36 | 54.87 |
| | ±0.14 | | ±3.77 | | | | ±2.09 | |
| $^{77}$Ir | 4.64 | 4.33 | 96.59 | 100.25 | – | – | 57.21 | 59.62 |
| | ±0.19 | | ±3.86 | | | | ±2.29 | |
| $^{78}$Pt | 4.72 | 4.80 | 102.36 | 109.63 | – | – | 60.45 | 64.65 |
| | ±0.19 | | ±4.09 | | | | ±2.42 | |
| $^{79}$Au | 4.97 | 5.24 | 113.25 | 118.01 | – | – | 65.02 | 70.18 |
| | ±0.20 | | ±4.53 | | | | ±2.6 | |
| $^{80}$Hg | 5.60 | 5.77 | 121.37 | 128.13 | – | – | 75.88 | 75.75 |
| | ±0.22 | | ±4.87 | | | | ±3.04 | |
| $^{81}$Tl | 6.09 | 6.35 | 129.99 | 138.80 | – | – | 83.42 | 81.90 |
| | ±0.24 | | ±5.16 | | | | ±3.34 | |
| $^{82}$Pb | 7.52 | 7.02 | 143.22 | 149.69 | – | – | 94.91 | 88.11 |
| | ±0.30 | | ±5.75 | | | | ±3.8 | |
| $^{83}$Bi | 7.08 | 7.64 | 153.51 | 160.81 | – | – | 101.80 | 94.97 |
| | ±0.28 | | ±5.98 | | | | ±4.07 | |
| $^{90}$Th | 11.68 | 13.2 | 237.10 | 244.56 | 52.26 | 64.11 | 144.87 | 149.90 |
| | ±0.58 | | ±11.90 | | ±4.18 | | ±7.24 | |
| $^{92}$U | 13.88 | 15.4 | 269.52 | 287.19 | 65.44 | 77.06 | 155.23 | 159.11 |
| | ±0.69 | | ±16.25 | | ±5.25 | | ±7.76 | |

agree within (3.6–18.8%) with the theoretical values calculated by Cohen [48] using energy-loss Coulomb-repulsion perturbed-stationary-state relativistic theory (ECPSSR). The empirical values of the $L$ shell average fluorescence yields are smaller than the theoretical values except for $Z \geq 82$. The main reason of these was thought because some transitions could not be observed.

The disagreement between the experimental and theoretical results can either be due to same systematic error in the experimental measurements or to an error in the calculated values of the physical parameters ($\sigma_{Li}$ and/or $F_{ny}$) used to evaluate the theoretical $L$ X-ray production cross-sections. Besides, in order to reduce the statistical error, two spectra were recorded for each target. The uncertainty in the area of the $L$ X-ray peak was evaluated by weighted method. The $L_i$ $(i = \ell, \eta, \alpha_{1,2}, \beta_{1,2,6,9,10,15,17}, \gamma_{1,2,3,5})$ photopeak areas were separated by fitting the measured spectra with multi-Gaussian functions plus polynomial backgrounds using software program.

TABLE I (cont.)

| Element | $\sigma_{L_{2\gamma}}$ ($\gamma_{1.5}$) | | $\sigma_{L_{1\beta}}$ ($\beta_{9.10}$) | | $\sigma_{L_{1\gamma}}$ ($\gamma_{2.3}$) | | $\sigma_{L_{2\eta}}$ ($\eta$) | |
|---|---|---|---|---|---|---|---|---|
| | Exp. | Theor. | Exp. | Theor. | Exp. | Theor. | Exp. | Theor. |
| $^{75}$Re | 10.74 | 10.23 | – | – | – | – | – | – |
| | ±0.43 | | | | | | | |
| $^{76}$Os | 11.02 | 11.40 | – | – | – | – | – | – |
| | ±0.44 | | | | | | | |
| $^{77}$Ir | 12.44 | 12.77 | – | – | – | – | – | – |
| | ±0.54 | | | | | | | |
| $^{78}$Pt | 13.98 | 14.14 | – | – | – | – | – | – |
| | ±0.56 | | | | | | | |
| $^{79}$Au | 14.68 | 15.72 | – | – | – | – | – | – |
| | ±0.59 | | | | | | | |
| $^{80}$Hg | 15.13 | 17.29 | – | – | 3.22 | 2.32 | 2.60 | 2.05 |
| | ±0.61 | | | | ±0.19 | | ±0.16 | |
| $^{81}$Tl | 17.21 | 19.10 | – | – | 3.29 | 2.41 | 2.66 | 2.22 |
| | ±0.69 | | | | ±0.2 | | ±0.16 | |
| $^{82}$Pb | 19.44 | 20.95 | – | – | 3.30 | 2.66 | 3.52 | 2.39 |
| | ±0.78 | | | | ±0.2 | | ±0.21 | |
| $^{83}$Bi | 20.04 | 23.02 | – | – | 4.11 | 2.92 | 3.23 | 2.58 |
| | ±0.80 | | | | ±0.25 | | ±0.19 | |
| $^{90}$Th | 34.86 | 40.85 | 12.26 | 15.71 | 6.07 | 5.42 | 4.20 | 4.18 |
| | ±1.74 | | ±1.12 | | ±0.55 | | ±0.38 | |
| $^{92}$U | 41.25 | 44.46 | 18.23 | 24.30 | 8.11 | 7.02 | 4.63 | 4.47 |
| | ±2.06 | | ±1.64 | | ±0.73 | | ±0.42 | |

As a result, the present agreement between the theoretical and present experimental values leads to the conclusion that the data presented here are important for qualitative and quantitative element analysis using XRF and electron-probe microanalysis (EPMA) techniques because of their use in applied fields. For this reason, to obtain a more definite conclusion on $L$ X-ray cross-sections, more experimental and theoretical data are clearly needed. Besides, in many element analysis works, generally $L$ X-ray peaks have been used by researchers.

TABLE II

Average $L$ shell fluorescence yields.

| Element | $\varpi_L$ | | | |
|---|---|---|---|---|
| | Experimental | Theoretical | | |
| | | [46] | [47] | [48] |
| $^{75}$Re | 0.235±0.014 | – | 0.308 | 0.280 |
| $^{76}$Os | 0.252± 0.015 | – | 0.320 | 0.293 |
| $^{77}$Ir | 0.255±0.015 | 0.300 | 0.332 | 0.305 |
| $^{78}$Pt | 0.258±0.015 | 0.320 | 0.344 | 0.318 |
| $^{79}$Au | 0.272±0.019 | 0.389 | 0.356 | 0.332 |
| $^{80}$Hg | 0.292±0.020 | 0.380 | 0.369 | 0.345 |
| $^{81}$Tl | 0.314±0.022 | 0.430 | 0.381 | 0.359 |
| $^{82}$Pb | 0.345±0.029 | 0.360 | 0.393 | 0.372 |
| $^{83}$Bi | 0.369±0.031 | 0.400 | 0.406 | 0.385 |
| $^{90}$Th | 0.451±0.036 | 0.488 | – | 0.475 |
| $^{92}$U | 0.481±0.038 | 0.510 | 0.515 | 0.499 |

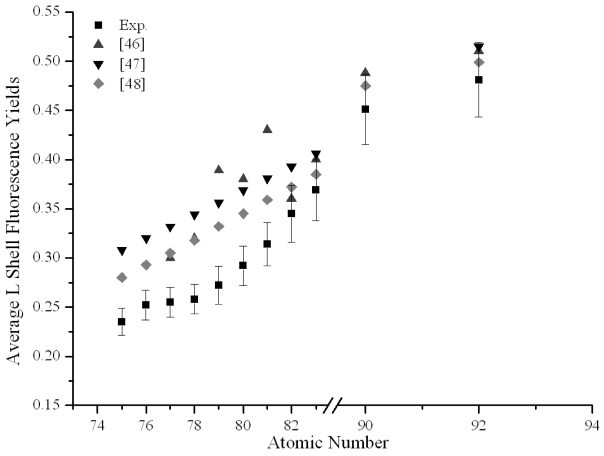


Fig. 3. Average $L$ shell fluorescence yields versus atomic number.

## References

[1] S.K. Arora, K.L. Allawadhi, B.S. Sood, *J. Phys. B, At. Mol. Phys.* **14**, 1423 (1981).

[2] K. Shatendra, K.L. Allawadhi, B.S. Sood, *Phys. Rev. A* **31**, 2918 (1985).

[3] S. Puri, B. Chand, M.L. Garg, N. Singh, J.H. Hubbell, P.N. Trehan, *X-Ray Spectrom.* **21**, 171 (1992).

[4] M. Şahin, L. Demır, Ö. Söğüt, M. Ertuğrul, O. İçelli, *J. Phys. B, At. Mol. Opt. Phys.* **33**, 93 (2000).

[5] R. Durak, Y. Özdemir, *Spectrochim. Acta B* **55**, 177 (2000).

[6] M. Ertuğrul, *J. Phys. B, At. Mol. Opt. Phys.* **34**, 2081 (2001).

[7] M. Ertuğrul, *Nucl. Instrum. Methods Phys. Res. B* **179**, 459 (2001).

[8] E. Tıraşoğlu, U. Çevik, B. Ertuğral, Y. Atalay, A.İ. Kopya, *Radiat. Phys. Chem.* **60**, 11 (2001).

[9] A. Karabulut, A. Gürol, G. Budak, R. Polat, *Eur. Phys. J. D* **21**, 57 (2002).

[10] M. Ertuğrul, *Anal. Chim. Acta* **491**, 239 (2003).

[11] P. Singh, M. Sharma, J.S. Shahi, D. Mehta, N. Singh, *Nucl. Instrum. Methods Phys. Res. B* **211**, 33 (2003).

[12] A. Kaya, M. Ertugrul, *J. Electron Spectrosc.* **130**, 111 (2003).

[13] A. Küçükönder, B.G. Duru, Ö. Söğüt, E. Büyükkasap, *J. Rad. Nucl. Chem.* **260**, 89 (2004).

[14] S. Singh, D. Mehta, M.L. Garg, S. Kumar, N. Singh, P.C. Mangal, P.N. Trehan, *J. Phys. B, At. Mol. Opt. Phys.* **20**, 3325 (1987).

[15] N. Singh, R. Mittal, K.L. Allawadhi, B.S. Sood, *J. Phys. B, At. Mol. Opt. Phys.* **20**, 5639 (1987).

[16] K.S. Mann, K.S. Kahlon, H.S. Aulakh, N. Singh, R. Mittal, K.L. Allawadhi, B.S. Sood, *Pramana* **37**, 293 (1991).

[17] K.S. Mann, N. Singh, Raj Mittal, B.S. Sood, K.L. Allawadhi, *X-ray Spectrom.* **23**, 208 (1994).

[18] A. Kumar, S. Puri, J.S. Shahi, M.L. Garg, D. Mehta, N. Singh, *J. Phys. B, At. Mol. Opt. Phys.* **34**, 613 (2001).

[19] R.R. Garg, S. Puri, S. Singh, D. Mehta, J.S. Shahi, M.L. Garg, N. Singh, P.C. Mangal, P.N. Trehan, *Nucl. Instrum. Methods Phys. Res. B* **72**, 147 (1992).

[20] S. Puri, D. Mehta, N. Singh, P.N. Trehan, *Phys. Rev. A* **54**, 617 (1996).

[21] O. Doğan, Ö. Şimşek, Ü. Turgut, M. Ertuğrul, *Phys. Scr.* **56**, 580 (1997).

[22] D.V. Rao, R. Cesareo, G.E. Gigante, *Nucl. Instrum. Methods Phys. Res. B* **83**, 31 (1993).

[23] D.V. Rao, R. Cesareo, G.E. Gigante, *X-Ray Spectrom.* **22**, 401 (1993).

[24] K.A. Al-Saleh, N.S. Saleh, *Radiat. Phys. Chem.* **54**, 117 (1999).

[25] A.C. Mandal, M. Sarkar, D. Bhattacharya, P. Sen, *Nucl. Instrum. Methods Phys. Res. B* **174**, 41 (2001).

[26] A.C. Mandal, S. Santra, D. Mitra, M. Sarkar, D. Bhattacharya, *Nucl. Instrum. Methods Phys. Res. B* **234**, 176 (2005).

[27] S. Fast, J.L. Flinner, A. Glick, F.W. Inman, L. Oolman, C. Pearson, D. Wickelgren, *Phys. Rev. A* **26**, 2417 (1982).

[28] S. Fazinic, I. Bogdanovic, M. Jaksic, I. Orlic, V. Valkovic, *Nucl. Instrum. Methods Phys. Res. B* **94**, 363 (1994).

[29] T. Papp, J.L. Campbell, *Nucl. Instrum. Methods Phys. Res. B* **114**, 225 (1996).

[30] V.J. Kennedy, A. Augusthy, K.M. Varier, P. Magudapathy, K.G.M. Nair, B.B. Dhal, H.C. Padhi, *Nucl. Instrum. Methods Phys. Res. B* **161-163**, 196 (2000).

[31] C. Tang, Z. An, Z. Luo, M. Liu, *J. Appl. Phys.* **91**, 6739 (2002).

[32] Y. Wu, Z. An, M.T. Liu, Y.M. Duan, C.H. Tang, Z.M. Luo, *J. Phys. B, At. Mol. Opt. Phys.* **37**, 4527 (2004).

[33] Y. Wu, Z. An, Y.M. Duan, M.T. Liu, C.H. Tang, *J. Phys. B, At. Mol. Opt. Phys.* **40**, 735 (2007).

[34] J. Semaniak, J. Braziewicz, M. Pajek, T. Czyzewski, T. Glowacka, M. Jaskola, M. Haller, R. Karschnick, W. Kretschmer, Z. Halabuka, D. Trautmann, *Phys. Rev. A* **52**, 1125 (1995).

[35] A.B. Hallak, *J. Phys. B, At. Mol. Opt. Phys.* **31**, 4573 (1998).

[36] Y.C. Yu, A.R. Azordegan, H.L. Sun, J.L. Duggan, F.D. McDaniel, E.K. Lin, C.W. Wang, G. Lapicki, *Nucl. Instrum. Methods Phys. Res. B* **150**, 27 (1999).

[37] R. Mehta, N.K. Puri, Ajay Kumar, A. Kumar, B.P. Mohanty, P. Balouria, I.M. Govil, M.L. Garg, T. Nandi, A. Ahamad, G. Lapicki, *Nucl. Instrum. Methods Phys. Res. B* **241**, 63 (2005).

[38] G. Apaydın, E. Tıraşoğlu, *Nucl. Instrum. Methods Phys. Res. B* **246**, 303 (2006).

[39] M.J. Berger, J.H. Hubbell, *XCOM: Photon Cross-Sections on a Personal Computer* (version 1.2), NBSIR85-3597, National Bureau of Standards, Gaithersburg, MD, USA, for version 3.1, 1999, see http://physics.nist.gov/.

[40] J.H. Scofield, Lawrence Livermore Laboratory (UCRL), Vol. 51326, 1973.

[41] B. Ertuğral, G. Apaydin, H. Baltas, U. Çevik, A.İ. Kobya, M. Ertuğrul, *Spectrochim. Acta B* **60**, 519 (2005).

[42] M.O. Krause, *J. Phys. Chem. Ref. Data* **8**, 307 (1979).

[43] S. Puri, D. Metha, B. Chand, N. Singh, J.H. Hubbell, P.N. Trehan, *Nucl. Instrum. Methods Phys. Res. B* **83**, 21 (1993).

[44] J.H. Scofield, *At. Data Nucl. Data Tables* **14**, 121 (1974).

[45] J.H. Scofield, *Phys. Rev.* **179**, 9 (1969).

[46] W. Bambynek, B. Crasemann, R.W. Fink, H.U. Freund, H. Mark, C.D. Swift, R.E. Price, P.V. Rao, *Rev. Mod. Phys.* **44**, 716 (1972).

[47] I.V. Mitchell, K.M. Barfoot, *Nucl. Sci. Appl.* **1**, 99 (1981).

[48] D.D. Cohen, *Nucl. Instrum. Methods Phys. Res. B* **22**, 55 (1987).